DEPARTMENT OF PHYSICS, UNIVERSITY OF JYVÄSKYLÄ
RESEARCH REPORT No. 1/1976

STUDIES OF 14 MeV NEUTRON ACTIVATION CROSS SECTIONS WITH SPECIAL REFERENCE TO THE CAPTURE REACTION

BY
MIKKO VALKONEN

Academic Dissertation
for the Degree of
Doctor of Philosophy

Jyväskylä, Finland
March 1976

ISBN 951-677-620-5

DEPARTMENT OF PHYSICS, UNIVERSITY OF JYVÄSKYLÄ
RESEARCH REPORT No. 1/1976

STUDIES OF 14 MeV NEUTRON ACTIVATION CROSS SECTIONS WITH SPECIAL REFERENCE TO THE CAPTURE REACTION

BY

MIKKO VALKONEN

Academic Dissertation
for the Degree of
Doctor of Philosophy

To be presented, by permission of the
Faculty of Mathematics and Natural Sciences
of the University of Jyväskylä,
for public examination in Auditorium II-212 of the
University on April 3, 1976, at 12 o'clock noon.

Jyväskylä, Finland
1976

URN:ISBN:978-951-39-9829-5
ISBN 978-951-39-9829-5 (PDF)
ISSN 0075-465X

Jyväskylän yliopisto, 2023

ISBN 951-677-620-5

Preface

It is a pleasure for me to express my sincere gratitude to my teacher, Professor J. Kantele; he offered a wealth of ideas, continuous encouragement and support during the course of studies involved in the preparation of this thesis. Thanks are also due to him for excellent working conditions at the Department of Physics of the University of Jyväskylä.

My gratitude is due to Professor M. Karras and Professor I. Bergqvist for excellent facilities for work they placed at my disposal at the Department of Nuclear Technology of the University of Oulu and at the Department of Nuclear Physics of the University of Lund.

To my co-authors Mr. G. Magnusson, Phil Mag., Dr. R. Rieppo and Mr. J. K. Keinänen, Phil.Lic., I am greatly indebted.

Special thanks are due to Mr. R. Komu, Mr. A. Lyhty and Mr. P. Paljakka for technical assistance. May I extend my thanks to all my other colleagues, as well.

I am obliged to Professor P. Lipas for checking the manuscript. Finally, I am indebted to Mrs. Terhi Räsänen, who skilfully typed the manuscript.

My gratitude is also due to Suomen Kulttuurirahasto, to the Finnish Academy of Sciences, to Leo and Regina Wainstein Foundation, to Oskar Öflunds Stiftelse, to A. Nyyssönen Foundation, to NORDITA and to the Rector of the University of Jyväskylä, Professor I. S. Louhivaara, for financial support.

Jyväskylä, February 1976

Mikko Valkonen

Contents

STUDIES OF 14 MeV NEUTRON ACTIVATION CROSS SECTIONS WITH SPECIAL REFERENCE TO THE CAPTURE REACTION

Abstract

Uncertainties in 14 MeV neutron activation cross-section measurements, especially in neutron capture, have been studied systematically. The sources of error in the activation method have been pointed out. Some methods for the correct measurements of the neutron cross sections by the activation method have been developed.

A number of new cross-section values have been determined and compared with other experimental and theoretical results. Discrepancies between former activation capture results and results of the spectrum method for 14-15 MeV neutrons have been removed with the help of the correct results measured in the present work.

1. Introduction

During the past two decades, a large number of activation cross sections for 14-15 MeV neutrons have been measured[1] which have resulted in cross-section systematics[2-15]. These measurements have been especially popular in laboratories having simple neutron generators well suited to this type of experiment. On the other hand, the activation method appears to be a straightforward way to measure total cross sections which can be compared directly with the predictions of the various theoretical models[16-37].

Sometimes, however, the suitability of the models is difficult to estimate because the results from different measurements of the same cross section may disagree very badly [1,9,10,11,12,26,27,30,32,33,43]. Therefore, a systematic study of the reasons for the differences of the various cross-section results for 14-15 MeV neutrons was called for. This was one of the reasons for starting the present work; also, more specifically, it was considered important to find out why, in the capture reaction measurements, the results of the activation method[1,43] and the spectrum method[9,24,26,27,32,35,41] differed systematically.

The mass-number dependence of the activation results seemed to show clearly that shell effects are present in spite of the highly excited state of the nucleus involved[29].

The systematics of the results of the spectrum method demonstrated, however, that the mass number dependence of

the capture cross section was very weak in the mass region $A \gtrsim 50$ and all cross sections had a nearly constant value ($\simeq 1$ mb). Physically, this discrepancy would mean a difference in the decay mode of the highly excited state of the nucleus and also different descriptions of the neutron capture reactions.

According to the activation results, the states initially populated should decay mainly via transitions through unbound states when the target nucleus is between the neutron shell closures and, if the target nucleus is in the vicinity of the neutron shell closures, mainly directly to the bound states through an E1 transition. The behaviour of the results of the spectrum method indicates, on the other hand, that the neutron capture reaction proceeds in every case through an E1 transition[14].

The importance of the present study was also emphasized since highly excited states reached in the neutron capture reaction at 14-15 MeV energy are overlapping with the giant dipole resonance states.

By examining the experimental cross-section results in the literature, it was established that the activation results scattered more than the results of the spectrum method. Halpern, quoted in ref.[9], suggested that differences between the activation results and the results of the spectrum method are caused by inaccuracies in the activation method, because of the secondary neutrons produced by the reactions (n,2n), (n,n') etc. in the target or itssurroundings.

In the present work, reasons for the inaccuracies of the cross section results in the activation method for 14-15 MeV neutrons have been systematically studied and several new methods for "correct" measurements of activation cross sections developed[44-46]. Some cross sections for the reactions (n,2n), (n,p), (n,α) and (n,γ) at the neutron energy of 14-15 MeV have been measured using the new methods. The present results have been compared with the results of other measurements and with the results of the latest models.

The present results of the neutron capture cross sections agree well with the results of the spectrum method. This also confirms that the "shell effects" exhibited by the previous activation capture data are due to experimental errors.

The inaccuracies in the activation method and the methods for minimizing them are studied in section 2. The correct cross section measurements and the present cross section results are given in section 3. A comparison between experimental and theoretical results is described in section 4. Special attention has been paid to the study of the capture cross sections.

The present work has been carried out during the years 1970-1975, partly at the Department of Physics, University of Jyväskylä, Finland, partly at the Department of Nuclear Technology, University of Oulu, Finland, and

partly at the Department of Nuclear Physics, University of Lund, Sweden. Most of the results have already been published in earlier papers[12,44-46,50,57,85]. This work is a summary based mainly on the following publications:

1. M. Valkonen and J. Kantele:
   The role of target geometry in 14 MeV neutron capture cross section measurements
   Nucl. Instr. and Meth. 103, 549 (1972)
   https://doi.org/10.1016/0029-554X(72)90014-6
2. J. Kantele and M. Valkonen:
   Mass number dependence of activation capture cross sections for 14 MeV neutrons
   Phys. Letters 39 B, 625 (1972)
   https://doi.org/10.1016/0370-2693(72)90014-7
3. M. Valkonen and J. Kantele:
   A simple two-detector method for precision inter-comparisons of source strengths
   Nucl. Instr. and Meth. 99, 25 (1972)
   https://doi.org/10.1016/0029-554X(72)90129-2
4. J. Kantele and M. Valkonen:
   Corrections for positon annihilation in flight in nuclear spectrometry
   Nucl. Instr. and Meth. 112, 501 (1973)
   https://doi.org/10.1016/0029-554X(73)90169-9
5. P. Holmberg, R. Rieppo, A. Hietanen and M. Valkonen:
   Activation cross-sections for 14.7 MeV neutrons on natural zinc
   ISBN 951-42-0045-4 Report 25 (1972)
6. P. Holmberg, R. Rieppo, J.K. Keinänen and M. Valkonen:
   Activation cross-sections for 14.7 MeV neutrons on chromium
   J. inorg. nucl. Chem. 36, 715 (1974)
   https://doi.org/10.1016/0022-1902(74)80798-0
7. R. Rieppo, J.K. Keinänen and M. Valkonen:
   Activation cross-sections for 14.7 MeV neutrons on natural germanium, to be published in J. inorg. nucl. Chem. (1976)
   https://doi.org/10.1016/0022-1902(76)80439-3

2. Sources of error in the activation method

During the past twenty years, neutron cross section measurements have been almost exclusively carried out by the activation method[7]. In principle, the activation method may seem to be a simple and straightforward way to measure 14-15 MeV neutron cross sections. However, correct and reliable results are not so easily reached since high-quality versatile measurement equipment and knowledge of the details of the method, and especially of the sources of errors, are needed.

Discrepancies in the previous activation cross-section results were mainly due to the following:

(a) Errors due to uncertainty in neutron energy

(b) Effects of impurities in the sample

(c) Secondary neutrons from (n,2n), (n,n') and (n,pn) reactions in the activation target or surrounding materials which have a dicisive effect upon the capture cross section measurements

(d) Uncertainties in cross sections of reactions used as comparison standards in the determination of the neutron flux

(e) Strong energy dependence of the reactions involved

(f) Uncertainties in connection with the chemical separation procedure of the sample

(g) Uncertainties in the measuring geometry of the activities and trivial errors due to the equipment

(h) Errors due to uncertainties in detection efficiency of counters used in gross-beta measurements and in the analysis of the resulting decay curves

(i) Errors or uncertainties in the decay schemes used in the analysis of the induced activities

(j) In cross-section determination of the reaction (n,2n), the positon annihilation peak is often used without correction for positon annihilation in flight

2.1. Limitations of the activation method

The activation method cannot be used in measurements of the total cross sections if the half-life of the final nucleus is not suitable, or, when using a natural target, the reaction to be studied and some other reaction have the same result nucleus. If the disturbing reaction has a negligible cross section compared with the one studied, the effect of this disturbance can be taken into account, and the activation method can be used also in these cases. The capture cross sections for 14-15 MeV neutrons can be determined by the activation method and with natural targets only for the heaviest stable isotope

of an element because of the reaction (n,2n) which is typically about 100-1000 times more probable than the capture reaction[1].

2.2. Sources of error in the activation

2.2.1. Determination of the neutron energy

In practice, 14-15 MeV neutrons are produced in the reaction $T(D,n)^4He$. If the reaction angle of the neutrons striking the samples can be correctly fixed in the determination of the energies of these DT-neutrons[47], only a small uncertainty due to retarded deuterons using thick tritium targets[47] is present. Knowledge of neutron energies and energy distributions is important because of the strong energy dependence of many cross sections[48]. Though neutron capture cross sections are nearly independent of the neutron energy in the energy region 14-15 MeV, the neutron energies must be known accurately because of the energy dependence of the standard reactions. If a tritium target is used for a long time, deuterons can be stuck in the target, and this may result in the $D(D,n)^3He$ reaction, which produces neutrons with an energy of about 2.5 MeV. In cross-section measurements of the

reactions (n,2n), (n,p) and (n,α), DD-neutrons can be usually neglected because of the rather large negative Q-values of these reactions[49].

In capture cross-section measurements of 14-15 MeV neutrons, the DD-neutrons may easily spoil the results because of their much greater capture cross sections. Therefore production of DD-neutrons must be minimized by using the same tritium target only for a few activations.

2.2.2. Impurities of the sample materials

In the published cross-section results, the information on sample materials has often been limited to the comments "natural targets" or "enriched targets". That is sufficient if the sample materials have had a high degree of purity. However, natural targets often contain a small amount of the element with the next atomic number.

Other impurities in small quantities do not usually cause difficulties if a Ge(Li) detector with a high resolution is used. However, in every case, all gamma peaks and half-lives in the spectra should be identified.

2.2.3. Activation geometry; secondary neutrons

Because of neutron scattering[48], materials between the tritium target and the activation target, as well as

the mass of the activation target, cause small uncertainties in the neutron energy in cross-section measurements of the reactions (n,2n), (n,p) and (n,α). In accurate measurements, the materials mentioned above and the size of the sample must therefore be minimized.

The most important sources of error in the previous neutron capture cross-section measurements by the activation method are due to too massive target heads of the neutron generators and too large activation targets, which give rise to secondary neutrons from the reactions (n,2n), (n,n') etc.

Besides the mass, also the geometry of the target head has an influence upon the production of the secondary neutrons. In the present work, the suitability of various materials for the target head has been examined by calculating the flux of the induced secondary neutrons as compared to the primary neutron flux. The primary neutrons pass through 5 mm thick layers of different materials. These materials were Perspex, aluminium, iron, copper, cadmium, tin and lead.

The results of these calculations are presented in table 1 which also shows the cross sections[1)] and the Q-values[48)] of the reactions inducing secondary neutrons and densities and molecular weights of the materials.

Table 1. Calculated flux of the secondary neutrons compared with the primary flux. The primary neutrons are assumed to pass through 5 mm thick layers of Perspex, aluminium, iron, copper, cadmium, tin and lead. In column 1, the molecular weights and densities (kg/m^3) of the materials are given. The coss sections and Q-values of the reactions which produce secondary neutrons are shown in columns 2 and 4, respectively. The underlined numbers refer to isomeric states.

Material	σ(mb)	F_{sec}/F_{pr} (%)	Q(MeV)
Perspex:			
$C_5H_8O_2$			
M ≃ 80			
ρ = 1.19 ^{2}H	$\sigma(n,2n)$ = 192		- 2.2
^{12}C	$\sigma(n,2n)$ = 6		-18.7
^{16}O	$\sigma(n,n'p)$ = 15		-12.6
Al:		0.24	
M = 27.0	$\sigma(n,2n)$ ≤ 0.17		-13.1
ρ = 2.70	$\sigma(n,n'p)$ = 78		- 8.3
Fe:		3.86	
M = 55.8			
ρ = 7.86			
^{56}Fe	$\sigma(n,2n)$ = 470		-11.2
	$\sigma(n,n'p)$ = 35		-10.2
Cu:		5.94	
M = 63.5			
ρ = 8.92			
^{63}Cu	$\sigma(n,2n)$ = 500		-10.8
^{65}Cu	$\sigma(n,2n)$ = 980		- 9.9

Table 1 continue

Cd:		4.44	
M = 112.4			
ρ = 8.64			
^{110}Cd	$\sigma(n,2n) = 1000$		- 9.9
$^{111-114}$Cd	$\sigma(n,2n) \simeq 900$		$\simeq$ - 9.0
^{116}Cd	$\sigma(n,2n) = 820$		- 8.7
	670		- 8.9
Sn:		3.50	
M = 118.7			
ρ = 5.75			
$^{112-120}$Sn	$\sigma(n,2n) \simeq 1200$		$\simeq$ - 9.3
^{122}Sn	$\sigma(n,2n) = 1450$		- 8.8
Pb:		3.49	
M = 207.2			
ρ = 11.34			
^{206}Pb	$\sigma(n,2n) = 1100$		- 9.1
^{207}Pb	$\sigma(n,2n) \simeq 1100$		- 6.7
^{208}Pb	$\sigma(n,2n) = 990$		- 8.4

On the basis of the results in table 1, aluminium was selected as the material for the target head. The first design of the target head, target head I, with water cooling is presented in fig. 1.

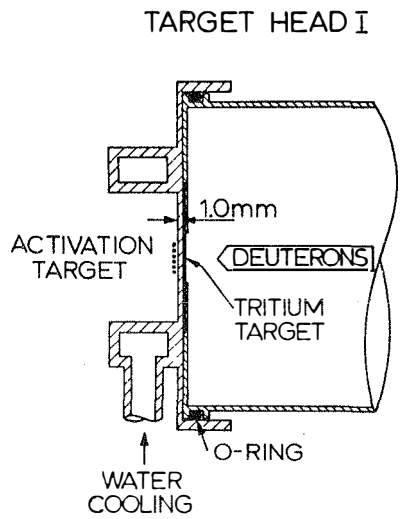

Fig. 1. Cross section of the target head I with water cooling. The material is aluminium.

Target head I is suitable for cross section measurements of the reactions (n,2n), (n,p) and (n,α).

The suitability of target head I for capture cross-section measurements was examined by inserting 5 mm thick slabs of different materials (mentioned in table 1) between the target head and a potassium iodide sample during the activation, and by determining the apparent total cross section for the reaction $^{127}I(n,\gamma)$ in every case. The results are presented in fig. 2.

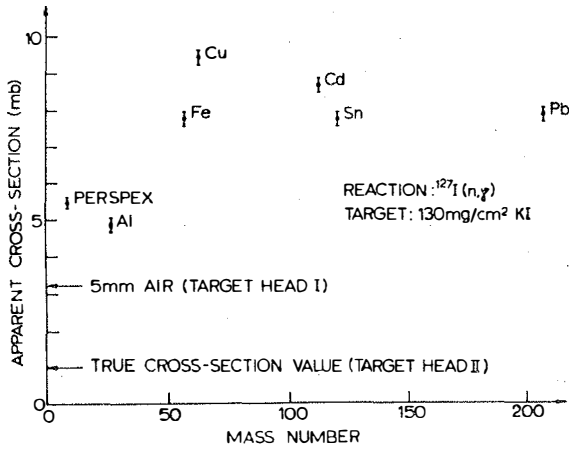

Fig. 2. The influence of 5 mm thick layers of various materials placed between target head I surface and a potassium iodide sample. The materials are listed in table 1. For comparison the correct cross-section value for the reaction $^{127}I(n,\gamma)$ from fig. 5 is also shown.

The main significance of these results for this work was the difference between 5 mm of air and 5 mm of

aluminium. This difference showed that target head I was still too massive for accurate measurements of the capture cross sections. Especially for the determination of capture cross sections, another target head, target head II with air cooling, was developed. This target head is presented in fig. 3.

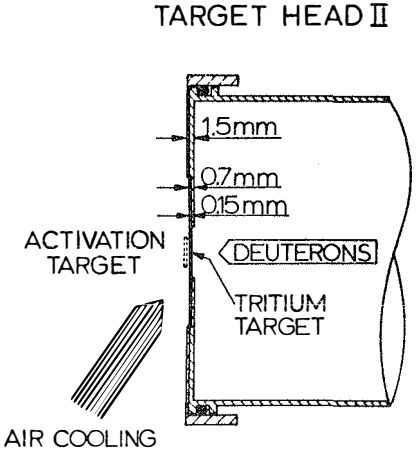

Fig. 3. Cross section of target head II with air cooling. The material is aluminium. The thin tritium target is deposited on a 0.025 mm thick copper backing. The aluminium foil between the activation target and the tritium target is only 0.15 mm thick in order to minimize the production of secondary neutrons.

In target head II, where the total mass has been minimized, neutrons penetrate a 0.025 mm thick copper backing of the tritium target and a 0.15 mm thick aluminium foil before hitting the sample. In the design of this target head, a sufficient mechanical strength required by the atmospheric pressure is achieved, while yet having a minimum amount of matter in the immediate vicinity of the targets.

In the present work the influence of the sample thickness on the capture cross-section results has been studied experimentally. The dependence of the apparent capture cross section on the thickness of the activation target measured with target head I in the reactions $^{81}Br(n,\gamma)$, $^{127}I(n,\gamma)$ and $^{170}Er(n,\gamma)$ is presented in fig. 4.

An interesting feature of fig. 4 is the much stronger dependence of the $^{81}Br(n,\gamma)$ cross section on the sample thickness as compared to the other cases. By investigating molecular weights[51], cross sections and Q-values[49] of the reactions inducing secondary neutrons, energy distributions of the induced secondary neutrons[16], and capture cross sections for thermal and low-energy neutrons[48], the stronger dependence of the $^{81}Br(n,\gamma)$ cross section can be qualitatively understood. Since the processes involved are rather complex and the experimental data are incomplete, it is hardly possible to carry out accurate quantitative calculations on the behaviour of the curves presented in fig. 4.

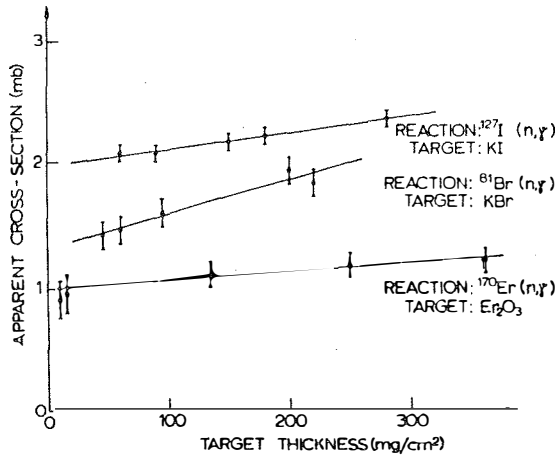

Fig. 4. Dependence of the apparent capture cross section on the thickness of the activation target in some cases (target head I).

The dependence on target thickness of the apparent cross section for the reaction $^{127}I(n,\gamma)$ (fig. 4) was remeasured in target head II geometry. The results shown in fig. 5, as compared with those in fig. 4, clearly demonstrate the great difference between the target heads I and II.

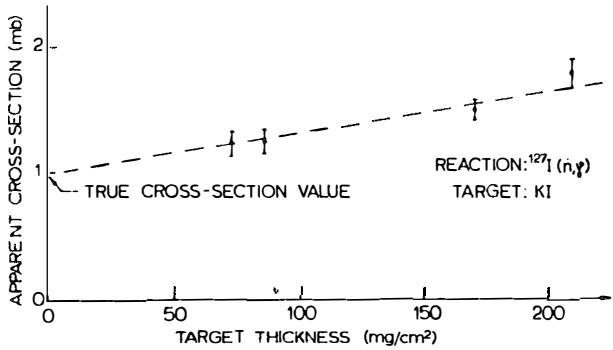

Fig. 5. Apparent total cross section for the reaction $^{127}I(n,\gamma)$ at 14.5 MeV mean neutron energy as a function of sample thickness. The contribution of the "massless" target head II to the cross-section values is estimated to be ≃ 0.1 mb.

The curve for the target thickness dependence of the apparent cross sections measured in a "massless" target head geometry (for example, in target head II geometry) is to be extrapolated to zero thickness of the target in order to exclude multiple reaction effects. Because the "massless" target head is not really massless, a small target head contribution correction must be made. In the target head II geometry, this correction was about 0.1 mb for $^{127}I(n,\gamma)$.

Similar curves for the thickness dependence of capture cross section were obtained by Ponnert, Magnusson and Berqvist[52] for $^{115}In(n,\gamma)^{116m}In$.

Devaney[53] has calculated multiple-reaction correction factors for contributions of large activation targets to capture cross sections. Since the processes involved are complex and the calculation method of Devaney rather simple, the results are less reliable than those obtained experimentally (see, for example, fig. 5).

2.2.4. Determination of the neutron flux

The most common standard reactions used to determine the neutron flux in the activation method are $^{27}Al(n,\alpha)$, $^{27}Al(n,p)$, $^{56}Fe(n,p)$, $^{63}Cu(n,2n)$ and $^{65}Cu(n,2n)$. Of course, the choice of the standards depends on the reactions to be studied and on the measurement equipment available. In general, at least two standard reactions should be used in order to eliminate the effects of variations of the neutron energy.

Because of uncertainties in the cross sections of the standard reactions[1], the ratios of the unknown and standard cross sections should also be reported. This would be of great help in later re-evaluations of the results after possible changes in the adopted values of the standards.

2.2.5. Stability of the neutron flux; activation time

An example of the influence of the instability of the neutron flux upon the results obtained by the activation method is given in fig. 6.

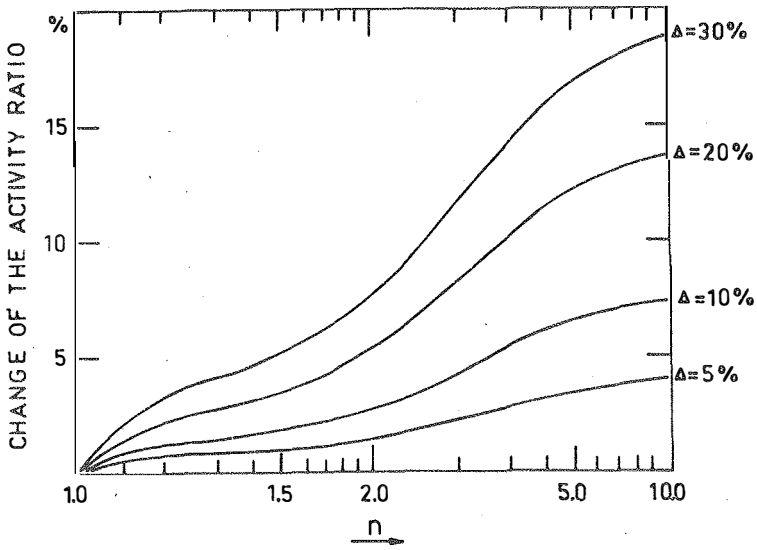

Fig. 6. Change of the ratio of two simultaneously induced activities when the neutron flux is during the first half of the activation period Δ% less and during the second half Δ% more than the mean value of the flux, as compared with the case of a constant flux. The change of the ratio is plotted as a function of the half-life of the standard activity. The activation period is taken as equal to the half-life of the activity studied; the half-life of the standard activity is n times this half-life.

The change of the ratio of the induced activities in fig. 6 show that an instability of the neutron flux must always be taken into account in a cross-section measurement by the activation method. In the present work, the variations of the neutron flux are followed and corrected for with the aid of neutron detectors. The necessary corrections can be made accurately by dividing the activation time into short periods and by detecting the number of neutron pulses during each period[54].

The activation time should be chosen separately in each case depending on the build-up factor of the reactions, the stability of the neutron flux and the total time available for the measurement.

2.3. Sources of error in the determination of the induced activities

2.3.1. General

Obviously the method of measurement of the activities must be chosen separately depending on the case. The main principle should be, however, to measure gamma-ray spectra, if possible, because of uncertainties in the

detection efficiency of β-counters used in gross-beta measurements and in the analysis of the spectra.

Beta-ray measurements are useful only in the cases in which the half-life of the activity to be determined differs much from the half-lives of the other activities induced in the activation target.

For several apparent reasons, the measurements of singles spectra is the simplest and the most reliable method to determine activities. Absorption corrections are connected with the experimental determination of efficiency curves for Ge(Li) detectors. Methods of determining the intensity of gamma peaks are well known, and so the main attention should be paid to the exact carrying out of these determinations.

In the present work, radiochemical methods were not needed consequently, large uncertainties often characteristic of these methods were avoided.

2.3.2. Geometry of the measurements; two-detector method

In measurements of direct gamma-ray spectra, there usually are no difficulties in the measurement geometry if the activities to be compared can be measured at the same time[55]. However, if the activities must be studied one after another, it is very important to use a geometry where both samples can be placed in the same place.

One of the latest solutions to this problem, a two-detector method, has been developed in the present work. The basic idea of the present method can be understood from figs. 7 and 8. The former figure shows two geometric arrangements which can be applied in comparing sources placed near the origin of either coordinate frame. In the latter figure, the relative counting rates of the two detectors are shown as functions of the x coordinate of a ^{137}Cs source (2 mm in diameter) moved along the x axis. When the source is near the origin, the changes in the two counting rates compensate each other fairly accurately, as can be seen from the curve which represents their average. For example, the average value at x=1 mm coincides with the "center" value N_o (which represents the ideal case of no geometric uncertainty) within 1 ‰, although each of the counting rates N_A and N_B differs from N_o by more than 2 ‰.

If the source is not very close to the origin, or if the x coordinate is not known or cannot be determined accurately, the mere average counting rate $1/2(N_A+N_B)$ may not give sufficiently accurate or reliable information. This difficulty can be overcome with the aid of simple correction curves of the type shown in fig. 9. In this figure, the deviation of the mean counting rate from N_o is plotted against the ratio N_A/N_B (or N_B/N_A).

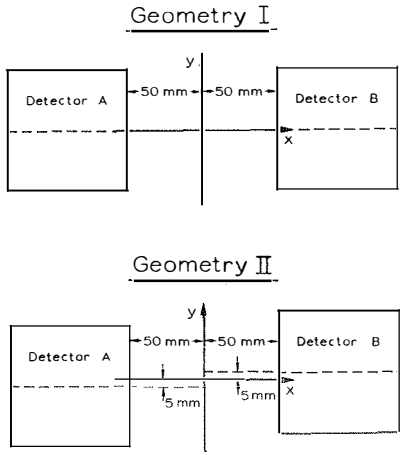

Fig. 7. Two geometric arrangements suitable for precision intercomparisons of source strengths. In both cases, the detectors are placed in the same horizontal plane; in geometry I, the axes of the detectors coincide; in geometry II the axis of detector A lies at y = -5 mm and the axis of detector B at y = +5 mm. The former geometry applies to measurements of point or line sources placed on the x axis, while the latter geometry allows some uncertainty in the source position in both x and y directions. Consequently, geometry II is also suited to precision comparisons of disc (or "spot") sources. The detectors employed are 7.6 cm by 7.6 cm NaI(Tl) crystals.

Consequently, if a small source is placed somewhere on the x axis between the detectors, the sum and the ratio of the two measured counting rates can be used in an obvious way to compute the "true" counting rate N_0, in principle to any desired accuracy. This statement also holds for a line source coinciding with the x axis. Uncertainties due to statistics, peak area determinations, absorption corrections etc. are not considered in the present discussion. It is assumed that the efficiency and correction curves can be represented by second-order polynomials, which is well justified (cf. caption of fig. 8).

In many experiments it may not be possible to place the source accurately on the x axis, or even the dimension of the source may require that the effect of nonzero y or z coordinates be taken into account. Fig. 10 shows the variation of the counting rate of detector B with the y coordinate in geometry I for x = +5, 0 and -5 mm. The y dependence of the counting rate is obviously much weaker than the x dependence; for example, $|y| < 1.5$ mm corresponds to an efficiency decrease of 1 %. However, if a two-dimensional ("spot") source is being studied, or if the source position is not accurately known, geometry I may not be satisfactory. In such case geometry II can be used as it helps to compensate for position uncertainties in two dimensions.

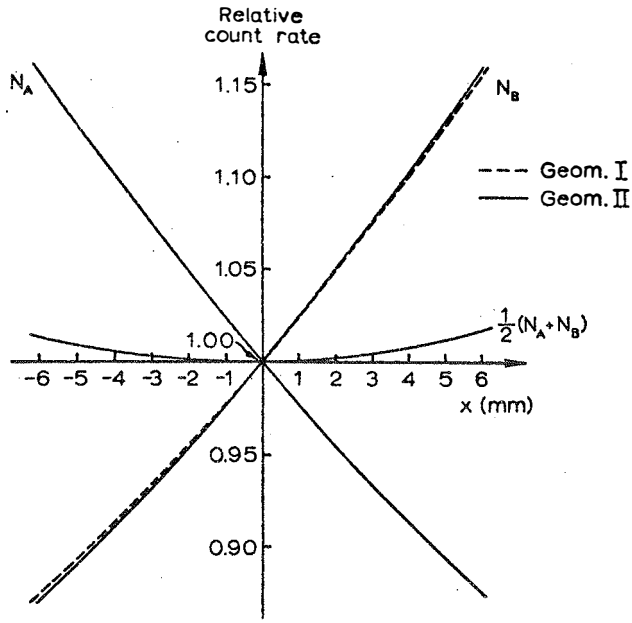

Fig. 8. Relative counting rates N_A and N_B of the detectors shown in fig. 7 vs the position of the source on the x axis (y=0). Note that the curves for both geometries (shown for detector B only) are almost identical. In the measurements a ^{137}Cs source was employed, and the curves represent the second-order polynomial fits to the data obtained. (Practically all of the experimental points and their limits of error lie within the drawn curves.) It is easy to see that the average counting rate $(1/2)(N_A+N_B)$ is fairly insensitive to changes in the x coordinate, especially at small values of x.

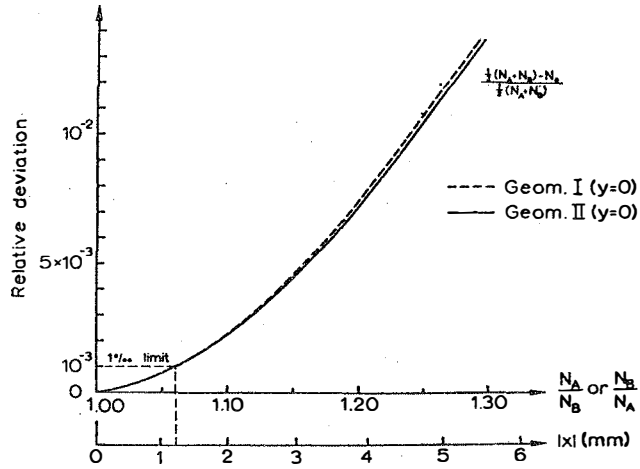

Fig. 9. Deviation of the mean counting rate $(1/2)(N_A+N_B)$ from the "center" counting rate N_O plotted vs the ratio N_A/N_B (or N_B/N_A). (At x=0, y=0, $N_A=N_B=N_O$.) These curves have been obtained directly from those of fig. 8 and correspond to the case y=0. With the aid of the above deviation curves, one can easily compute the "true" or "center" counting rate N_O from the measured N_A and N_B. It can be seen that, if the observed counting rates do not differ from each other, by more than 5 % (which corresponds to the case $|x| < 1$ mm), the mean values $(1/2)(N_A+N_B)$ deviates from N_O by less than 1 % . The x scale is shown in the figure for comparison only; in the actual correction procedure, no information on the x coordinate is needed.

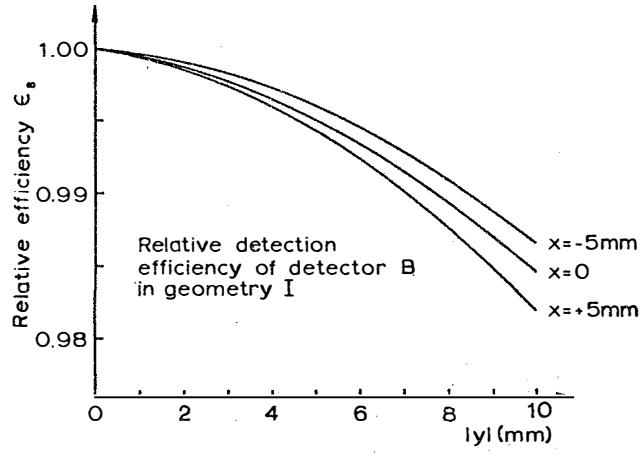

Fig. 10. Dependence of the detection efficiency (or counting rate) of detector B on the y coordinate in geometry I.

With the aid of fig. 10, it can be understood that the misalignment of the detector axes in geometry II has the effect that, if $|y| < 5$ mm, any step in the $\pm x$ or $\pm y$ directions gives rise to an increase in the counting rate of one of the detectors and to a simultaneous decrease in the counting rate of the other one. Therefore, a correction method along the lines described

above can be expected to apply in this case, too. It turns out, in fact, that the very same simple method illustrated in fig. 9 gives fairly good results also in the two-dimensional case. In other words, both x and y corrections can reasonably well be performed merely by using the sum and the ratio of N_A and N_B together with the correction curve of fig. 9. The accuracy of the simple correction method as applied in the xy plane is illustrated in fig. 11 which shows the errors made when the source is placed at some points near the origin. The usefulness of the method in measurements with two-dimensional sources is apparent.

It is clear that the present type of arrangement can be absolutely calibrated accurately with the aid of sources with known disintegration rates. The detectors do not need to be identical; for example, the method has been used successfully with two Ge(Li) detectors of different types.

The correction curve to be employed must of course be determined for each geometry and γ-ray energy used in the source strength determinations. However, if the energies to be studied are not very low, the relative efficiency (or counting rate) curves of the type illustrated in fig. 8 depend only weakly on the γ-ray energy. Estimates based on known efficiency curves

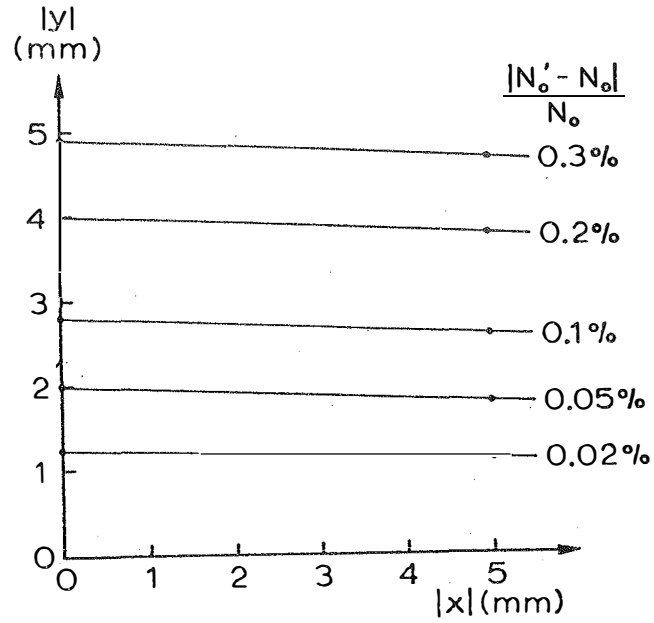

Fig. 11. Limits of error of the simple correction method illustrated in fig. 9, as applied in geometry II where the x and y coordinates are both allowed to change. N_0' is the "center counting rate" obtained from the actual rates N_A and N_B with the aid of one of the correction curves of fig. 9. The points indicated by dots are calculated on the basis of the curves in fig. 10. The points have been simply connected with straight lines to give a picture of the accuracy of the method. As an example, if a disc source of 5 mm in diameter is placed (horizontally) at the center of the system within a radial accuracy of 2 mm, the equivalent counting rate N_0 can be determined with an accuracy of better than 0.05% (if uncertainties due to vertical position, absorption and other factors can be neglected).

show, for example, that the curves in the energy range of 0.5 to 2 MeV corresponding to the x coordinate range of fig. 8 do not deviate by more than 0.5 % from the curves determined for the ^{137}Cs γ-ray energy of 661 keV. In the range of 1 to 2 MeV, all curves agree to within $\pm$ 1 % with the curves determined for the energy of 1.5 MeV.

2.3.3. Gamma-ray intensity ratios; corrections for positon annihilation in flight

Cross-section results by the activation method are directly proportional to the intensity values of the observed gamma lines and therefore a good knowledge of decay schemes is necessary for good cross-section results. Previously, discrepancies and often errors of decay schemes gave rise to the scattering of the cross-section results. The rapid development of the knowledge of decay schemes during the last few years can be seen by looking at results given in the two commonly used handbooks, Table of Isotopes[59] and Nuclear Data Tables[58]. In some cases the intensity values given in these books differ by more than a factor of ten. Differences in the cases of "well-known" nuclei are not so large, but there are 5-10 % differences in the intensity values of standard activities, too.

In cross-section measurements of the reaction (n,2n) the 511 keV positon annihilation peaks are often used to measure the positon activities. This is a useful method if the intensity of positons is well-known and if the corrections for positon annihilation in flight are made.

In the present work, the probability of positon annihilation in flight was studied both theoretically and experimentally. Calculations were made using the theories of Jaeger and Hulme[38] and of Bethe[39] for single- and two-quantum annihilation in flight, respectively, and the Fermi beta-decay theory[40]. Confirmation of the theoretical basis employed was obtained by comparing total absolute probabilities for annihilation in flight of ^{62}Cu positons in Perspex, copper, cadmium and lead, using a new differential method[46]. The agreement with the theory was found to be excellent.

The decrease of the annihilation peak by annihilation in flight[46] depends on the end-point energy of positons and on the annihilation material as shown in fig. 12.

The curves in fig. 12 have been determined on the assumptions that the atomic number of the positon emitter is $Z_o = 29$ and the positon transition is allowed. The curves can be used in all cases because the effect of the variation of Z_o is very small.

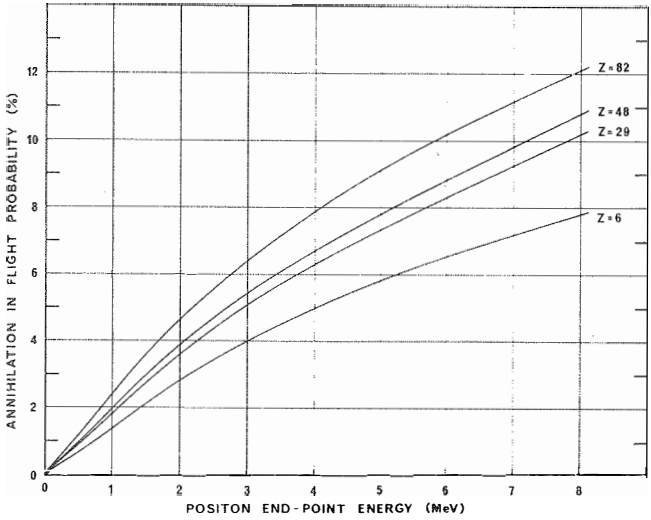

Fig. 12. Calculated average probabilities of annihilation in flight (single- plus two-quantum) of positons of allowed continuous spectra. The curves for the different stopping materials are calculated for the parent atomic number $Z_o = 29$. However, the dependence on Z_o is very weak and can be neglected in all practical cases. The curve labelled Z = 6 is actually calculated for Perspex $(C_5H_8O_2)_n$.

2.4. Estimation of total errors in activation cross-section results

When known quantities of materials have been activated and the induced activities determined, the cross section can be calculated in a straightforward way. These calculations are based on the fact that the induced activity is equal to the measured activity when the activities are normalized to the same instant of time. In the present work, the normalizing point is in every case the end of the activation period.

The ratio of the cross section to be determined, σ_t, and the standard cross section σ_n is given by the formula

$$(a)\quad \frac{\sigma_t}{\sigma_n} = \frac{M_t}{M_n} \times \frac{m_n}{m_t} \times \frac{p_n}{p_t} \times \frac{1-e^{-\lambda_n t_s}}{1-e^{-\lambda_t t_s}} \times \frac{A_{pt}}{A_{pn}}$$

$$\times \frac{(DT)_t}{(DT)_n} \times \frac{E_{pn}}{E_{pt}} \times \frac{p'_n}{p'_t} \times \frac{\lambda_t}{\lambda_n} \times \frac{1-e^{-\lambda_n t_{mn}}}{1-e^{-\lambda_t t_{mt}}}$$

$$\times \frac{e^{\lambda_t t_{ot}}}{e^{\lambda_n t_{on}}} \times \frac{(Abs)_t}{(Abs)_n} \times \frac{(summ)_t}{(summ)_n} \quad ,$$

where the subscript t refers to the "unknown" activity and n to the standard one (in the following, i = t or n) and

M_i = molecular weight of the material,

m_i = mass of the sample material,

p_i = percent abundance of the target isotope,

$\lambda_i = \frac{\log_e 2}{(T_{1/2})_i}$, with $T_{1/2}$ the half-life of the resulting activity,

t_s = activation time,

A_{pi} = area of the gamma peak,

$(DT)_i$ = dead-time correction,

E_{pi} = detection (photopeak) efficiency of the gamma ray,

p'_i = percent gamma-ray intensity,

t_{mi} = measuring time,

t_{oi} = waiting time (from normalizing point to starting point of measurement),

$(Abs)_i$ = absorption correction,

$(summ)_i$ = summing correction.

In a beta measurement E_{pi} must be replaced by the efficiency of the beta counter, incorporating the corrections for self absorption and backscattering from the backing of the sample.

In cross-section measurements of the reaction (n,2n) where the activities are determined from the annihilation peak of positons, corrections for annihilation in flight must be made in formula (a), too.

The total error in the activation cross section results from the uncertainties in several terms in formula (a). The most important contributions to the total error

are due to the following factors: uncertainties of the standard reactions (subsection 2.2.4), uncertainty in the measuring geometry (subsection 2.3.2), dead-time corrections, statistical uncertainty of the peaks in the gamma-ray measurements, uncertainties in the gamma-ray intensities (which have a great effect), and the failure of the correction for positon annihilation in flight (subsection 2.3.3). In beta measurements, the efficiency corrections and self absorption of the samples must also be taken into account.

In the examination above, it is assumed that the neutron flux is constant during the activation. The effects on the final cross-section results due to variations of the neutron flux are discussed in subsection 2.2.5.

In measurements of the neutron capture cross section, also secondary neutrons with significant effects must be taken into account. The exact determination of the effects of the secondary neutrons presuppose often measurements with special geometries (subsection 2.2.3).

3. "Correct" cross-section measurements

In the present work, a number of cross-section results of the reactions (n,2n), (n,p), (n,α) and (n,γ) for 14-15 MeV neutrons has been determined using the methods of chapter 2. In these measurements special attention has been paid to the elimination of the effects of the sources of error and to the accuracy of the required corrections. The experiments have been carried out using Ge(Li) detectors and modern electronic equipment[44-46,52,56-57]. Activation targets have been natural samples with purity degrees better than 99.9 percent. Only in the case of $^{103}Rh(n,\gamma)$ leading to two ^{204}Rh isomers[59], a plastic scintillation detector was used[45] and the beta counting performed. The reliability of this measurement was checked by following the decay of the β spectra.

3.1. Measurements and results of the reaction (n,2n)

The cross section of the reaction (n,2n) has been measured for ^{39}K, ^{50}Cr, ^{63}Cu, ^{64}Zn, ^{70}Ge, ^{69}Ga, ^{79}Br, ^{107}Ag, ^{141}Pr and ^{144}Sm by using 14.7 MeV neutrons. The reactions $^{27}Al(n,p)$, $^{27}Al(n,\alpha)$ and $^{63}Cu(n,2n)$ have been used as standard reactions with adopted cross-section values of 65 ± 5 mb[48], 115 ± 5 mb[48] and 535 ± 25 mb, respectively.

In the following table 2 half-lives of the induced activities[58] are shown, together with the intensities and end-point energies of the positon spectra[58,59] and the present cross-section results.

Table 2. The present cross-section results ($\sigma \pm \Delta\sigma$) of the reaction (n,2n) at 14.7 MeV mean neutron energy.

Reaction	Induced activity			Cross section (mb)	
	$T_{1/2}$ a)	I_{β^+}(%) a)	T_o(MeV) a)	σ(n,2n)	$\Delta\sigma$(n,2n)
$^{39}K(n,2n)^{38g}K$	7.71^m	100	2.68	4.7	0.55
$^{50}Cr(n,2n)^{49}Cr$	41.9^m	93	1.54	24	5
$^{63}Cu(n,2n)^{62}Cu$	9.7^m	97.5	2.91	535	25
$^{64}Zn(n,2n)^{63}Zn$	38.6^m	100	2.34	190	20
$^{69}Ga(n,2n)^{68}Ga$	68.3^m	88	1.90	820	80
$^{70}Ge(n,2n)^{69}Ge$	39.2^h	34	1.22	575	130
$^{79}Br(n,2n)^{78}Br$	6.4^m	92	2.55	955	55
$^{107}Ag(n,2n)^{106g}Ag$	24.1^m	70	1.96	700	70
$^{141}Pr(n,2n)^{140}Pr$	3.39^m	50	2.32	1590	160
$^{144}Sm(n,2n)^{143}Sm$	8.9^m	50	2.4	1250	150

a) From refs. 58 and 59.

3.2. Measurements and results of the reactions (n,p) and (n,α)

The cross section of the reaction (n,p) have been measured for ^{52}Cr, ^{53}Cr, ^{54}Cr, ^{64}Zn, ^{66}Zn, ^{67}Zn, ^{68}Zn, ^{70}Ge, ^{72}Ge, ^{73}Ge, ^{74}Ge and ^{76}Ge and the cross sections of the reaction (n,α) for ^{54}Cr, ^{68}Zn, ^{72}Ge and ^{74}Ge.

The neutron energy and the standard reactions were the same as those used in the cross-section measurements of the reaction (n,2n). In table 3 are given the half-lives of the final activities[58], the energies and intensities of the gamma peaks used in the determination of the activities[58], and the present cross section results.

3.3. Measurements and results of neutron-capture reactions

In the present work, the aim of the neutron capture cross-section measurements was to find the reasons for the differences between the results from the activation method[7] and the spectrum method[26]. When the reasons for the activation errors were discovered (see section 2 and ref. 45), the neutron capture cross section was measured for ^{51}V, ^{81}Br, ^{103}Rh, ^{127}I, ^{154}Sm, ^{160}Gd, ^{165}Ho and ^{170}Er at a neutron energy of 14.5 MeV.

Table 3. The present cross-section results of the reactions (n,p) and (n,α) at 14.7 MeV mean neutron energy.

Reaction	Induced activity			Cross section	
	$T_{1/2}$ a)	E_γ(keV) a)	I_γ(%) a)	σ	Δσ
$^{52}Cr(n,p)^{52}V$	3.75^m	1434	100	94	10
$^{53}Cr(n,p)^{53}V$	1.55^m	1006	89	40	7
$^{54}Cr(n,p)^{54}V$	55^s	835, 986	100, 82	15	4
$^{64}Zn(n,p)^{64}Cu$	12.71^h	511 A	38	211	20
$^{66}Zn(n,p)^{66}Cu$	5.1^m	1039	9	76	7
$^{67}Zn(n,p)^{67}Cu$	61.7^h	187	40	140	20
$^{68}Zn(n,p)^{68}Cu$	30^s	1078	95	11	2
$^{72}Ge(n,p)^{72}Ga$	14.2^h	834	95.6	42	4
$^{73}Ge(n,p)^{73}Ga$	4.9^h	297	87	16	3
$^{74}Ge(n,p)^{74}Ga$	8.25^m	598	87	12	1
$^{76}Ge(n,p)^{76}Ga$	27^s	563	66	3.1	1.5
$^{54}Cr(n,\alpha)^{51}Ti$	5.8^m	320	95	7	4
$^{68}Zn(n,\alpha)^{65}Ni$	2.56^h	1482	25.7	11	2
$^{72}Ge(n,\alpha)^{69m}Zn$	13.8^h	439	95	11	2
$^{74}Ge(n,\alpha)^{71m}Zn$	3.97^h	609	65	20	2

a) From ref. 58.

Differences between old results by the activation method and results by the spectrum method were most conspicuous in these cases[12].

In the following phase of the present work, all possible cases for capture reaction measurements in the region $N \gtrsim 28$ were examined in order to find the cases in which capture cross sections can be measured by the activation method with better accuracy than 20 per cent. It was supposed that the discrepancies due to efficiency corrections and standard cross sections are less than 5 per cent. In these investigations, special attention was paid to other reactions, to the accuracy of the decay schemes and to the requirements of sufficient counting statistics. The accuracy of the counting statistics depends mostly on the half-life of the resulting activity and the intensity of the observed gamma rays, the abundance of the target isotope, the available neutron flux and the total efficiency of the available detector. The results are presented in table 4.

In table 4, one can see that the number of suitable cases for capture cross section measurements using natural targets and the activation method is limited. The list in table 4 is still shorter if the available neutron flux is lower than the flux used in the first phase of the present work ($F \simeq 10^7 \ldots 10^8$ n/cm^{2}s).

Table 4. Suitable cases for capture cross-section measurements by the activation method.

Target		Induced activity			
Isotope	Abund. [a]	$T_{1/2}$ [b]	E (keV) [b]	I (%) [c]	m or g
^{51}V	99.76	3.77^{m}	1434	100	
^{55}Mn	100	2.587^{h}	846	99	
^{71}Ga	39.6	14.1^{h}	834	95.63	m+g
^{75}As	100	26.5^{h}	560	41.05	
^{82}Se	9.19	25.0^{m}	356	69.0	g
^{81}Br	49.46	35.3^{h}	777,554	83.3,70.5	m+g
^{89}Y	100	3.1^{h}	202	97	m
^{104}Ru	18.58	4.43^{h}	724	44.5	
^{130}Te	34.48	25^{m}	150	67.7	g
		30^{h}	774	46	m
^{127}I	100	25^{m}	443	20.5	
^{138}Ba	71.66	82.7^{m}	166	27.4	
^{139}La	99.911	40.2^{h}	487,1596	46.7,96.0	
^{154}Sm	22.71	23^{m}	104	72.5	
^{160}Gd	21.90	3.7^{m}	361	66.0	
^{170}Er	14.88	7.52^{h}	308	64.4	
^{176}Yb	12.73	1.9^{h}	150	17.2	
^{186}W	28.41	23.9^{h}	686,480	32.0,26.0	
^{193}Ir	62.7	17.4^{h}	329	13.0	m+g
^{197}Au	100	64.8^{h}	412	94.7	

a) From ref. 59.
b) From ref. 58.
c) From refs. 58 and 59.

Table 5. The present capture cross-section results and the laboratories in which the measurements were carried out.

Reaction	Cross section (mb)	(mb)	Laboratory
$^{51}V(n,\gamma)^{52}V$	0.60	0.15	Univ. of Jyväskylä
$^{81}Br(n,\gamma)^{82}Br$	0.9	0.3	- " -
$^{103}Rh(n,\gamma)^{104m}Rh$	2	0.5	- " -
$^{127}I(n,\gamma)^{128}I$	0.9	0.3	- " -
$^{154}Sm(n,\gamma)^{155}Sm$	0.9	0.3	- " -
$^{160}Gd(n,\gamma)^{161}Gd$	1.0	0.4	- " -
$^{165}Ho(n,\gamma)^{166}Ho$	2	0.5	- " -
$^{170}Er(n,\gamma)^{171}Er$	0.9	0.3	- " -
$^{176}Yb(n,\gamma)^{177}Yb$	1.0	0.3	Univ. of Oulu
$^{186}W(n,\gamma)^{187}W$	1.1	0.4	- " -

In addition to the cases mentioned before, the capture cross sections for ^{176}Yb and ^{186}W have been measured. All present neutron capture cross-section results are presented in table 5.

4. Comparison of experimental and theoretical cross-section results

4.1. Reactions (n,2n), (n,p) and (n,α)

The statistical theory[3,10,16,18,20,23,25,87] has been found most successful in explaining the reactions (n,2n), (n,p) and (n,α). According to this theory, the incident neutron gives rise to the formation of a compound nucleus which can decay through a number of different channels. The differences between the various statistical calculations are mainly due to the different formulae for the nuclear level density. An excellent review of the different models for the (n,2n) reaction is given in ref. 3.

The present measurements of the cross sections of the reactions (n,2n), (n,p) and (n,α) were limited to the regions A ≃ 40-150, A ≃ 50-80 and A ≃ 50-80, respectively.

From table 6a-c one can see that the agreement between the predicted and the experimental results is quite good except for the cases ^{64}Zn(n,2n), ^{64}Zn(n,p), ^{68}Zn(n,p) and ^{74}Ge(n,α). In the case of ^{64}Zn(n,2n), the present experimental result agrees very well with the theoretical result of Bormann et al.[3].

Lu and Fink[10] have calculated some (n,2n), (n,p) and (n,α) cross sections for medium-Z nuclei using in their

statistical model a constant-nuclear-temperature approximation for the level densities. The results of these calculations are rather similar to those presented above.

Table 6a. (n,2n) cross-section comparison for 14.7 MeV neutrons. All results are given in mb.

Target	Present experiment	Other exp. ref. 1.	Pearlstein theory ref. 25
^{39}K	4.7 ± 0.55^{g}	5.1^{g} 8.8^{g+m}	4.9
^{50}Cr	24 ± 5	29.2	49
^{63}Cu	535 ± 25	500	540
^{64}Zn	190 ± 20	155	280
^{69}Ga	820 ± 80	850	730
^{70}Ge	575 ± 130	606	460
^{79}Br	955 ± 55	930	960
^{107}Ag	700 ± 70^{g}	800	1410
^{141}Pr	1590 ± 160	1670	1820
^{144}Sm	1250 ± 150	1740^{g+m} 1200^{g}	1565

Table 6b. (n,p) cross-section comparison for 14.7 MeV neutrons. All results in mb.

Target	Present experiment	Other exp. ref. 1.	Levkovskii theory ref. 87
^{52}Cr	94 ± 10	110	80
^{53}Cr	40 ± 7	43	45
^{54}Cr	15 ± 4	-	25
^{64}Zn	211 ± 20	210	140
^{66}Zn	76 ± 7	72	57
^{67}Zn	140 ± 20	88	37
^{68}Zn	11 ± 2	20	24
^{72}Ge	42 ± 11	47	30
^{73}Ge	16 ± 3	71	21
^{74}Ge	12 ± 1	11.2	14
^{76}Ge	3.1 ± 1.5	-	6.6

Table 6c. (n,α) cross section comparison for 14.7 MeV neutrons. All cross section results in mb.

Target	Present experiment	Other exp. ref. 1.	Levkovskii theory ref. 87
^{54}Cr	7 ± 4	-	10
^{68}Zn	11 ± 2	26	9.6
^{72}Ge	11 ± 2^{m}	0.47	12
^{74}Ge	20 ± 2^{m}	28	5.6

4.2. Neutron capture

4.2.1. Comparison of experimental results

The present correct activation results, previous activation results and spectrum method results for neutron capture cross sections are shown in table 7.

The present activation results agree with the spectrum method results quite well, while the previous activation results are clearly in disagreement with other results.

4.2.2. Neutron capture theories

In the theoretical examinations of the capture cross sections for 14-15 MeV neutrons there are in principle three different models:

(1) The statistical model[16] in which the compound nucleus decays through the radiative channel and which is a direct extension of the thermal neutron capture theory.

(2) The direct capture model[17] where the incident neutron is captured directly into an empty bound single-particle orbit and the excess energy is emitted as a gamma ray.

Table 7. Comparison of experimental neutron capture cross-section results at 14-15 MeV energy.

Target	Spectrum (mb)	Present (mb)	Previous activation method (mb)
^{51}V	0.73 ± 0.15 [26]	0.60 ± 0.15	0.37 ± 0.06 [15]
^{81}Br	1.1 ± 0.3 [41]	0.9 ± 0.3	3.5 ± 0.8 [43]
^{103}Rh	0.75 ± 0.20 [32]	<2	13.8 [61], 14.0 ± 3.0 [15]
^{127}I	1.09 ± 0.08 [24]	0.9 ± 0.3	2.5 ± 0.5 [43]
^{154}Sm		0.9 ± 0.3	-
^{160}Gd	0.90 ± 0.06 [9]	1.0 ± 0.4	3.0 ± 1.0 [62], 18.5 ± 5.6 [43]
^{165}Ho	1.05 ± 0.06 [9]	<2	8.8 ± 0.6 [15], ≤ 9.45 [43], 6.87 ± 1.44 [60]
^{170}Er	-	0.9 ± 0.3	-
^{176}Yb	-	1.0 ± 0.3	-
^{186}W	0.93 ± 0.17 [63]	1.1 ± 0.4	4.0 ± 0.8 [43]

(3) The collective models[19,21,22,34,36,37] in which the incident neutron, when inelastically scattered into a single-particle orbit, excites the target nucleus into the giant dipole state which subsequently decays by gamma-ray emission.

4.2.2.1. Statistical capture model

The starting point for the study of the neutron capture cross sections according to the statistical theory is the formula

(a) $$\sigma(n,\gamma) = \sigma_n \cdot G_\gamma \quad ,$$

where σ_n is the overall cross section for the compound nucleus formation and G_γ is the decay probability of the compound nucleus through the capture channel.

Lane and Lynn[17] have derived for G_γ the form

(b) $$G_\gamma = \frac{\Gamma_\gamma}{(1+x)\Gamma_n} \quad ,$$

where Γ_γ is the width for gamma-ray emission to levels of the residual nucleus below the nucleon separation energy, Γ_n is the neutron emission width at excitation energy E^* of the compound nucleus, and x is a factor

which takes into account effects of reactions other than neutron emission in the decay of the compound nucleus.

In the determination of the neutron width and the total capture width, Lane and Lynn used Newton's expression[65] for the level density of the compound nucleus and the formula of Feshbach and Weisskopf[66] for the level density of the residual nucleus. Their formula for the neutron absorption cross-section was based on the work of Thomas[67], and in calculations of the photon absorption cross section they used a formula derived from the profile function of Cauchy.

Among later studies of neutron capture according to the statistical theory, the calculations of Cvelbar et al.[26] for theoretical analysis of the neutron capture spectra must be mentioned.

4.2.2.2. Direct capture model

In the capture reaction according to the direct capture theory, the incident nucleon is captured into an empty bound single-particle orbit and the excess energy is emitted. The study can be limited to electric dipole radiation because the probability of magnetic dipole radiation and quadrupole radiation is in most cases two or three orders of magnitude smaller.

In standard notation[16], the cross-section formula for direct neutron capture, where the incident neutron goes into the single-particle state with quantum numbers n, l and j, is given as[27]

$$\text{(a)}\quad \sigma^{D}_{nlj} = K \sum_{l'j'} G(l,j,l',j') \left|\langle M^{D}_{nljl'j'}\rangle\right|^{2} ,$$

where

$$\text{(b)}\quad K = \frac{8\pi z^{2} e^{3} M_{n} E_{\gamma}{}^{3}}{3A^{2} k' h^{5} c^{3}} ,$$

$$\text{(c)}\quad G(l,j,l',j') = \tfrac{1}{2}(1+l'+1)(2j+1)(2j+1) \begin{Bmatrix} 1 & l & l' \\ \tfrac{1}{2} & j' & j \end{Bmatrix},$$

$$\text{(d)}\quad \langle M^{D}_{nljl'j'}\rangle = \int_{0}^{\infty} \psi_{nlj}(r)\, r^{3} \psi_{l'j'}(r)\, dr .$$

Here M_n and k' are the reduced mass and the wave number of the incident neutron, respectively. E_γ is the energy of the emitted gamma ray; $E_\gamma = E+B_{nlj}$, where E is the energy of the incident neutron in the center-of-mass coordinate frame and B_{nlj} is the binding energy of the state with quantum numbers n, l and j. The quantum numbers l, l' and j, j' refer to the initial and final states of the neutron, and {} is a Racah 6j symbol. $\psi_{l'j'}(r)$ is the radial wave function

of the initial state of the neutron, normalized according to $\int_0^\infty (\psi_{l'j'}(r))^2 r^2 dr = 1$, and $\psi_{nlj}(r)$ is the radial wave function of the final state of the neutron. In equation (a) sums are taken over $l' = l \pm 1$ and $j' = j \pm 1$.

The formula (a) agrees with that of Lane and Lynn[17] for direct neutron capture, with the addition of the factor which takes into account the spin-orbit interaction between the initial and final states.

4.2.2.3. Collective capture models

The idea of interference between capture processes through direct capture and through the giant resonance was suggested by Ferrell[82] in 1962.

Partly on the basis of this idea, Brown[19], Lushnikov and Zaretsky[22] and Clement, Lane and Rook[21] derived each their own formula for the collective neutron capture cross section.

The basic idea is that the total transition amplitude is a sum of the transition matrix element for the direct capture and a transition matrix element for the semi-direct capture. Brown[19] suggested that the core and the valence neutron are involved in the inverse reaction to capture, the photonuclear reaction. The capture process corresponds to the case in which the valence neutron is excited. By using a simple schematic model for calculating the interaction between the valence neutron

and the core, and for calculating the total dipole operator of the system, Brown got the following expression for the capture cross section:

$$\text{(a)} \qquad (\sigma^{DSD}_{nlj})_B = F_B \sigma^{D}_{nlj} \quad ,$$

where

$$\text{(b)} \qquad F_B = 1 + \frac{(E_R - E_D)^{\frac{1}{2}} + 2(E_R - E_D)(E_\gamma - E_R)}{(E_\gamma - E_R)^2 + \frac{1}{4}\Gamma^2} \quad .$$

Here σ^{D}_{nlj} is the cross section for direct capture in accordance with equation 4.2.2.2 (a), E_R is the excitation energy of the giant dipole resonance (GDR), Γ is the width of the GDR, E_D is the mean value of the excitation energy of the undisturbed particle-hole dipole, and E_γ is the energy of the emitted gamma ray.

Lushnikov and Zaretsky[22] derived their capture cross-section formula by using the inverse reaction, i.e. the photonuclear reaction. The cross section for the photonuclear reaction in the region of the GDR was derived by them using the general Migdal theory[84] in which the nuclei are handled as a Fermi gas of the interacting quasiparticles. The cross section of the photonuclear reaction can be transformed into the cross section of the capture reaction by examining the inverse reactions

and summing the part of the direct reaction cross section. The formula of Lushnikov and Zaretsky is

$$(c) \qquad (\sigma^{DSD}_{nlj})_{LZ} = F_{LZ}\sigma^{D}_{nlj} \quad ,$$

where

$$(d) \qquad F_{LZ} = \frac{(E_o^2-E_\gamma^2)^2 + \Gamma_o^2 E_o^2}{(E_R^2-E_\gamma^2)^2 + \Gamma^2 E_R^2} \quad .$$

Here the rotation is the same as in (a) and (b), but Γ_o means the width of the GDR according to the noninteracting quasiparticle model.

Clement, Lane and Rook[21] supposed that a deformed optical potential with a particle-vibration coupling term can excite the collective vibrational states of the nucleus through the interaction between the incident neutron and the target nucleus. The formula for the collective neutron capture cross section can be derived by adding the particle-vibration contribution to the wave functions of the initial states in the direct capture cross section equation as a perturbing term and by using a sum rule in the calculation of the state functions. The result is

$$(e) \qquad (\sigma^{DSD}_{nlj})_{CLR} = F_{CLR} \cdot \sigma^{D}_{nlj} \quad ,$$

where

$$(f) \quad F_{CLR} = \left| 1 + \frac{1}{E_\gamma - E_R + \frac{1}{2}\Gamma} \cdot \frac{N(l+0.8)\hbar^2 V_l}{4A M_n E_R} \cdot \frac{\langle M^C_{nljl'j'} \rangle}{\langle M^D_{nljl'j'} \rangle} \right|^2$$

$$\langle M^C_{nljl'j'} \rangle = \int \psi_{nlj}(r) \left(-\frac{1}{U} \frac{dU}{dr}\right) r^2 \psi_{l'j'}(r) dr \ ,$$

U is the optical potential of the incident neutron and V_l is the strength of the particle-vibration coupling. Otherwise the notation is the same as in (a)-(d) and 4.2.2.2 (a)-(d).

The models of Brown[19], Clement, Lane and Rook[21], and the later models of Longo and Saporetti[36] and Potokar[34] are applications of the same basic idea and their differences appear only in the coupling interaction functions.

These differences in interactions between the incident neutron and the giant dipole excitation of the target nucleus can be better understood by writing the neutron capture cross section in terms of the direct capture cross section, σ^D_{nlj}, for the capture of a neutron width angular momentum quantum numbers l' and j' into a single-particle orbit with quantum numbers n, l and j, and an effective charge factor F_{eff}:

$$(g) \qquad \sigma^{DSD}_{nlj} = \sigma^{D}_{nlj} \cdot F_{eff} ,$$

where

$$(h) \qquad F_{eff} = \left| 1 - \frac{1}{E_R - E_\gamma - i\frac{\Gamma}{2}} \frac{\int \psi_{nlj}(r) h(r) \psi_{l'j'}(r) dr}{\int \psi_{nlj}(r)\, r\, \psi_{l'j'}(r) dr} \right|^2 .$$

Here $h(r)$ is the coupling interaction function which is proportional to the particle-vibration coupling, and which is just the factor responsible for the differences between the various formulations.

The formula of Brown[19] for $h(r)$ was

$$(1) \qquad h(r) = \Delta E \cdot r ,$$

where ΔE is the shift in energy of the dipole state from the unperturbed particle-hole energy.

Clement, Lane and Rook[21] described the polarization of the target nucleus differently by using a surface-peaked particle-vibration coupling,

$$(2) \qquad h(r) = \cancel{\text{const}} \frac{df(r)}{dr} ,$$

where $f(r)$ is the nuclear density form factor.

Longo and Saporetti[31,36] suggested a volume form for the coupling,

(3) $$h(r) = \text{const}\, r\, f(r) \ .$$

Zimanyi, Halpern and Madsen[37] had an expression

(4) $$h(r) = \text{const}\, \left(a\frac{df(r)}{dr} + bf(r)\right) \ ,$$

where the contributions of a surface-peaked coupling and a volume term have been included.

The latest expression for the coupling interaction functions in the neutron capture cross sections is due to Potokar[34]. Potokar proposed a complex neutron-nucleus coupling interaction which has a real part of volume form and an imaginary surface-peaked part,

(5) $$h(r) = \text{const}\, r\left(V_1 f(r) - iW_1 4b \frac{df(r)}{dr}\right).$$

This expression for the coupling function implies the inclusion in the reaction mechanism of more complicated nuclear excitations than the previous formulations.

4.2.3. Comparison of theoretical and correct experimental results of neutron capture cross sections

The calculated neutron capture cross-section results obtained with the theories mentioned in chapter 4.2.2 and compared with correct experimental results in table 8 and

Table 8. Comparison of the correct experimental results and results from the different theories for neutron capture cross sections.

Target	Model	Theory (μb) ref. 27	Exp. (μb) ref. 26
^{27}Al	St	330 a)	690±50 a)
	D	100 a)	500±20 c)
	DSD_B	410 a)	410±80
^{32}S	St	90	500±100
	D	130	
	DSD_B	380	
	DSD_C	274	
^{52}Cr	St	80	920±180
	D	220	
	DSD_B	864	
	DSD_{LZ}	540	
^{56}Fe	St	60	870±170
	D	134	
	DSD_B	1130	
	DSD_{LZ}	470	
^{127}I	St	0.01 a)	1130±130
	D	400 a)	1090±80 a)
	DSD	990 c)	900±300 b)

a) From ref. 24.

b) Present work.

c) From ref. 81.

in ref. 27. The aim of these comparisons has been to examine the general validity of the statistical model, direct capture model and collective models.

The results of the statistical model and the direct capture model disagree clearly with the experimental results. Both models give results which are too small, the results of the statistical theory by one or two orders of magnitude, and the results of the direct model by about a factor of 2 - 10. The results of the collective models agree with the experimental results reasonably well.

The following table 9 presents a more extended comparison between the results of the DSD models and the correct experiments in the region $A \gtrsim 30$.

The agreement is in general good between the total capture cross-section results shown in table 9. However, more exact examinations of the validity of the various collective model formulations using total capture cross sections are impossible. This is because the accuracy of the experimental total neutron capture cross-section results is quite poor and the differences between the results of the various DSD formulations are small. Besides, the DSD results are strongly dependent on the selection of the parameter values used in calculations and there are considerable uncertainties in the literature even in the values of the most crucial factors.

Table 9. Comparison of the results of the correct experiments and the DSD model for 14-15 MeV neutrons in the region $A \gtrsim 30$.

Target	DSD (μb)	Ref. theory	Correct act. and spectr. (μb)	Ref. exp.
^{27}Al	410	24	690 ± 50	24
	510	81	500 ± 20	81 a)
			410 ± 80	26
^{28}Si	414	30	640 ± 165	30
			470 ± 70	82
^{32}S	380	27	500 ± 100	26
^{50}Ti	390	81	450 ± 30	81 a)
^{51}V	430	29	730 ± 150	26
			600 ± 150	present a)
	500	81	490 ± 60	81 a)
^{52}Cr	800	29	920 ± 180	26
	864	27		
^{55}Mn	950	29	780 ± 160	26
^{56}Fe	960	29	870 ± 170	26
	1130	27		
^{59}Co	820	29	700 ± 150	26
	730	32	1020 ± 260	32
^{82}Se	650	29	870 ± 170	41

Table 9 continue

^{85}Rb	805	30	770±230	30
^{89}Y	1200	29		
	965	30	1020±280	30
	1050	79		
^{93}Nb	700	32	800±200	32
^{103}Rh	720	32	750±200	32
			<2000	present a)
	810	81	< 2000±800	81 a)
^{127}I	990	81	1130±130	41
			1090± 80	24
			900±300	present a)
			< 1380±350	81 a)
^{133}Cs	1415	33	1510±420	33
^{138}Ba	1000	29	1400±300	41
^{139}La	1300	29	1350±400	33
	1155	33		
	980	81	700±300	81 a)
^{140}Ce	1170	33	1260±360	33
	1300	79		
^{159}Tb	1300	33	1750±450	33
^{165}Ho	1000	29	1050± 60	9
			< 2000	present a)
^{208}Pb	950	29	980±60	9
	780	31	900±300	83

a) Correct activation method.

Some studies of the validity of various DSD formulations have been made by using reaction gamma-ray spectra and partial cross sections for gamma rays to single-particle states[78-80]. For example, in the case of the $^{208}Pb(n,\gamma)$ $g_{9/2}$ partial cross section, the volume term formulation gives a better agreement with experimental results[78] that does the surface-peaked formulation.

4.2.4. Mass-number dependence of 14-15 MeV neutron capture cross sections

The mass number dependence of 14-15 MeV neutron capture cross sections is shown in fig. 13. The dependence is weak and in the region $A \gtrsim 50$ the cross section results are about one mb. Figure 13 shows also that the previous result for this dependence, which implied shell effects, was incorrect.

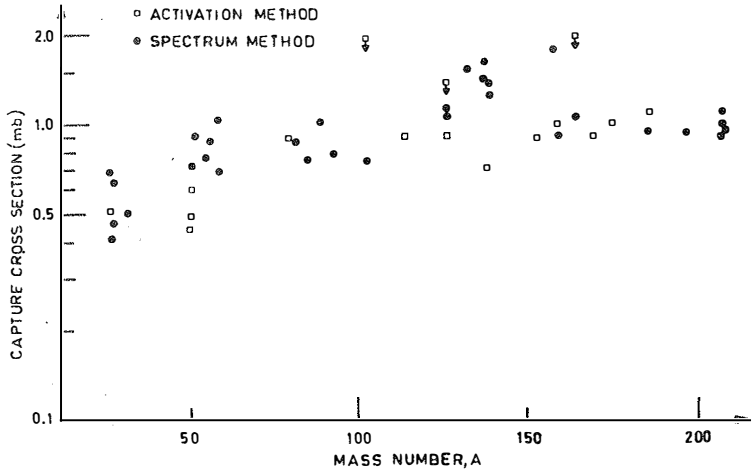

Fig. 13. Mass-number dependence of the correct experimental capture cross sections.

5. Conclusions

In the present work, the reasons for the inaccuracies of the activation cross-section results for 14-15 MeV neutrons were systematically studied and several new methods for "correct" measurements of activation cross-sections developed[44-46]. The accuracies of the activation results which can be reached using these methods are typically for the reactions (n,2n), (n,p) and (n,α) about 5-15 % and for the capture reaction 20-40 %. The poor accuracy of the capture cross sections is mainly due to the counting statistics because of low neutron fluxes and small samples.

The present experimental results of the reactions (n,2n), (n,p) and (n,α) agree quite well the latest results in most cases[11]. The statistical theory seems to be able to predict the results reasonably well, too.

In capture cross-section measurements by the activation method, the main attention must be paid to the corrections of the uncertainties due to the secondary neutrons. This has been demonstrated for the first time in the present work and its importance is apparent. The present results were confirmed by later work[52,86,88], in which, however, the total mass of the target heads used in the activations was larger, although the basic shape and the material were similar to ours.

The present results for the neutron capture cross sections agree well with the results obtained by the spectrum method. This agreement, together with the activation results of Rigaud et al.[81], indicate that most of the 14-15 MeV capture cross sections measured previously by the activation method are incorrect.

A comparison between the correct experimental and the theoretical results shows that one can obtain the best agreement using the DSD models. However, the general validity of the various DSD models cannot be evaluated using the total cross-section results because of the limited experimental accuracy and the strong dependence of the theoretical results on the parameters used.

References

1. H. Leppämäki and J. Kantele, Research Report No. 3/1970, Dept. of Physics, Univ. of Jyväskylä (1970)

2. M. Bormann, Nucl. Phys. 65, 257 (1965)

3. M. Bormann and B. Lammers, Nucl. Phys. A130, 195 (1969)

4. F. Manero, Inf. conf. on the study of nuclear structure with neutrons, Antwerp. p. 546 (1965) (North-Holland, Amsterdam, 1966)

5. P. Cuzzocrea and S. Notarrigo, see ref. 4, p. 544

6. P. Hille, Nucl. Phys. A107, 49 (1968)

7. G. Longo and F. Saporetti, Nucl. Phys. A127, 503 (1969)

8. Swapna Chatterjee and Aparesh Chatterjee, Nucl. Phys. A125, 593 (1969)

9. D. Drake, I. Bergqvist and D.K. MacDaniels, Phys. Letters 36B, 557 (1971)

10. W. Lu and R.W. Fink, Phys. Rev. C4, 1173 (1971)

11. S.M. Qaim, Nucl. Phys. A185, 614 (1972)

12. J. Kantele and M. Valkonen, Phys. Letters 39B, 625 (1972)

13. F. Cvelbar, A. Hudoklin and M. Potokar, Nucl. Phys. A138 412 (1969)

14. L. Nilsson and J. Eriksson, Phys. Letters 49B, 165 (1974)

15. J. Csikai, G. Petö, M. Buczko, Z. Miligy and N. Eissa, Nucl. Phys. A95, 229 (1967)

16. J.M. Blatt and V.F. Weisskopf, Theoretical nuclear physics (Wiley, New York, 1952)

17. A.M. Lane and J.E. Lynn, Nucl. Phys. 11, 646 (1959)

18. E.T. Bramlitt and R.W. Fink, Phys. Rev. 131, 2642 (1963)

19. G.E. Brown, Nucl. Phys. 57, 339 (1964)

20. H. Büttner, A. Lindner and H. Meldner, Nucl. Phys. 63, 615 (1965)

21. C.F. Clement, A.M. Lane and J.R. Rook, Nucl. Phys. 66, 273, 293 (1965)

22. A.A. Lushnikov and D.F. Zaretsky, Nucl. Phys. 66, 35 (1965)

23. M. Bormann, A. Behrend, I. Riehle and O. Vogel, Nucl. Phys. A115, 309 (1968)

24. H. Dinter, Nucl. Phys. A111, 360 (1968)

25. S. Pearlstein, Nuclear Data A3, 327 (1967)

26. F. Cvelbar, A. Hudoklin, M.V. Mihailović, M. Najžer and V. Ramšak, Nucl. Phys. A130, 401 (1969)

27. F. Cvelbar, A. Hudoklin, M.V. Mihailović, M. Najžer and M. Petrišič, Nucl. Phys. A130, 413 (1969)

28. G. Longo and F. Saporetti, Nucl. Phys. 56B, 264 (1968)

29. G. Longo and F. Saporetti, Nucl. Phys. A127, 503 (1969)

30. F. Rigaud, J. Roturier, J.L. Irigaray, G.Y. Petit, G. Longo and F. Saporetti, Nucl. Phys. A154, 243 (1970)

31. G. Longo and F. Saporetti, Nucl. Phys. A199, 530 (1972)

32. F. Rigaud, J.L. Irigaray, G.Y. Petit, G. Longo and F. Saporetti, Nucl. Phys. A173, 551 (1971)

33. F. Rigaud, J.L. Irigaray, G.Y. Petit, G. Longo and F. Saporetti, Nucl. Phys. A176, 545 (1971)

34. M. Potokar, Phys. Letters 46B, 346 (1973)

35. M. Potokar, A. Likar and F. Cvelbar, Proc. of sec. int. symp. on neutr. capt. gamma ray spectr. and rel. topics, p. 145, Petten (1974)

36. G. Longo and F. Saporetti, Phys. Letters 42B, 17 (1972)

37. J. Zimanyi, I. Halpern and V. Madsen, Phys. Letters 33B, 205 (1970)

38. J.C. Jaeger and H.R. Hulme, Proc. Cambridge Phil. Soc. 32, 158 (1936)

39. H.A. Bethe, Proc. Roy. Soc. (London) A150, 129 (1935)

40. Nuclear spectroscopy tables (eds. A.H. Wapstra, G.J. Nijgh and R. Van Lieshout; North-Holland Publ. Co., Amsterdam, 1959)

41. F. Cvelbar, A. Hudoklin and M. Potokar, Nucl. Phys. A158, 251 (1970)

42. G. Longo and F. Saporetti, Nucl. Phys. A199, 530 (1972)

43. J.L. Perkin, L.P. O'Connor and R.F. Coleman, Proc. Phys. Soc. 72, 505 (1958)

44. M. Valkonen and J. Kantele, Nucl. Instr. and Meth. 99, 25 (1972)

45. M. Valkonen and J. Kantele, Nucl. Instr. and Meth. 103, 549 (1972)

46. J. Kantele and M. Valkonen, Nucl. Instr. and Meth. 112, 501 (1973)

47. J. Kukkonen, pro gradu, Univ. of Jyväskylä, (1969) unpubl.

48. M.D. Goldberg et al. , Neutron cross sections, Vol. I-IIC, BNL-325 (1966)

49. N.B. Core and A.H. Wapstra, Nucl. Data Tables 11, 127 (1972)

50. P. Holmberg, R. Rieppo, A. Hietanen and M. Valkonen, ISBN 951-42-0045-4 (1973)

51. R.F. Weast et al., Handbook of Chemistry and Physics (The Chemical Rubber Co., Cleveland, Ohio, 1964)

52. K. Ponnert, G. Magnusson and I. Bergqvist, Physica Scripta 10, 35 (1974)

53. J. Denavay, Phys. Rev. Letters 29, 1567 (1972)
J. Denavay, Nucl. Sci. and Eng. 51, 272 (1973)

54. G. Magnusson, private communication (1975)

55. T. Komppa, Phil. Lic. thesis, Univ. of Jyväskylä, (1969) unpubl.

56. H. Helppi, Thesis for doctor degree, Univ. of Jyväskylä, (1974) unpubl.

57. R. Rieppo, J. Keinänen and M. Valkonen, to be publ. in J. inorg. Chem. (1976)

58. W.W. Bowman and K.W. MacMurdo, Nucl. Data Tables, Vol. 13, No. 2-3 (1974)

59. C.M. Lederer, J.M. Hollander and I. Perlman, Table of Isotopes, 6 th. ed. (J. Wiley, New York, 1967)

60. H.O. Menlove, K.L. Coop, H.A. Grench and R. Sher, Phys. Rev. 163, 1299 (1967)

61. J. Csikai, J. Bacso and A. Daroczy, Nucl. Phys. 41, 316 (1963)

62. R.G. Wille and R.W. Fink, Phys. Rev. 118, 242 (1960)

63. G.E. Brown, Unified theory of nuclear models, p. 29 (North-Holland Publ. Co., Amsterdam, 1964)

64. G. Petö et al. , Int. Symp. on Neutr. induced React., Smolenice, Czechoslovakia (1964)

65. T.D. Newton, Can. J. Phys. 34, 804 (1956)

66. H. Feshbach and V.F. Weisskopf, Phys. Rev. 76, 1550 (1949)

67. R.G. Thomas, Phys. Rev. 97, 224 (1955)

68. J.K. LeCouteur and J.M. Lang, Nucl. Phys. 13, 32 (1959)

69. G.S. Mani, M.A. Melkanoff and I. Iori, Rapport CEA, No. 2380 (1963)

70. E. Erba, U. Faccini and E. Saetta-Menichella, Nuovo Cimento 22, 1237 (1961)

71. E. Saetta-Menichella, F. Tonolini and L. Tonolini-Severgnini, Nucl. Phys. 51, 449 (1964)

72. U. Fano, NSA-NRC-1133 (1964)

73. A.G.W. Cameron, Can. J. Phys. 36, 1040 (1958)

74. L. Rosen, J.G. Beery and A.S. Goldhaber, Ann. of Phys. 34, 96 (1965)

75. B. Grimeland, E. Kjellsby and J. Vincs, Phys. Rev. 137, 878 (1965)

76. K. Okamoto, Phys. Rev. 110, 143 (1958)

77. J.M. Wyckoff, B. Ziegler, H.W. Koch and R. Uhlig, Phys. Rev. 137, 576 (1965)

78. I. Bergqvist, Proc. of sec. int. symp. on neutron capt. gamma ray spectr. and rel. topics, p. 199, Petten (1974)

79. A. Lindholm, L. Nilsson, I. Bergqvist and B. Pålsson, Proc. of sec. int. symp. on neutron capt. gamma ray spectr. and rel. topics, p. 239, Petten (1974)

80. L. Nilsson, A. Lindholm and I. Bergqvist, Proc. of sec. int. symp. on neutron capt. gamma ray spectr. and rel. topics, p. 222, Petten (1974)

81. F. Rigaud, M.G. Desthuilliers, G.Y. Petit, J.L. Irigaray, G. Longo and F. Saporetti, Proc. of sec. int. symp. on neutron capt. gamma ray spectr. and rel. topics, p. 233, Petten (1974)

82. R.A. Ferrell, Charlottesville Conf., 1962

83. I. Bergqvist, D.M. Drake and D.K. McDaniels, Nucl. Phys. A191, 641 (1972)

84. A.B. Migdal, Theory of finite Fermi systems and characteristics of atomic nuclei, Nauka, Moscow (1965)

85. P. Holmberg, R. Rieppo, J.K. Keinänen and M. Valkonen, J. inorg. nucl. Chem. 36, 715 (1974)

86. F. Rigaud, private communication in Asilomar, 1973

87. V.N. Levkovskii, Soviet journal of Nucl. Phys. 18, 361 (1974)

88. J. Vuletin, P. Kulicšič and N. Cindro, Lett. Nuovo Cimento 10, 1 (1974)

Jyväskylän yliopiston monistuskeskus
Jyväskylä 1976